Physica **76** (1974) 585–608

THE PRESSURE BROADENING OF THE ROTATIONAL RAMAN LINES OF HYDROGEN ISOTOPES

R.A.J. KEIJSER*, J.R. LOMBARDI, K.D. VAN DEN HOUT, B.C. SANCTUARY and H.F.P. KNAAP

Kamerlingh Onnes Laboratorium der Rijksuniversiteit Leiden, Leiden, Nederland
(Communication No. 408*c*)

Received 13 February 1974

Synopsis

The pressure broadening of the rotational Raman lines at room temperature is investigated for the hydrogen isotopes. For H_2, measurements have been carried out as a function of ortho–para composition. Evidence has been found that the contribution of resonance collisions to the widths of some of the Raman lines exceeds 40%. The results are compared with theoretical calculations.

1. *Introduction.* In the spectrum of the light scattered from dilute gases consisting of linear molecules, a series of equidistant lines is observed at both sides of the elastically (Rayleigh) scattered light. These lines correspond to spectroscopic transitions between the rotational states of the molecules. The selection rules for such transitions are $\Delta j = j_f - j_i = \pm 2$, where j_i and j_f denote the initial and final states of a transition. The lines are known as the rotational Raman lines. The rotational Raman scattering as well as the depolarized Rayleigh scattering ($\Delta j = 0$) (discussed in refs. 1 and 2) originates from the anisotropic part of the molecular polarizability, $\alpha_{\parallel} - \alpha_{\perp}$.

From a study of the pressure or collisional broadening of the Raman lines information can be obtained about the different types of collision processes that occur between nonspherical molecules. Such information can be used for a determination of the nonspherical part of the intermolecular potential.

In the pressure broadening of rotational Raman lines both energetically inelastic and energetically elastic collisions play a role[3,4]). Inelastic collisions give rise to spectral line broadening because a change of j upon collision interrupts the radiation process. The elastic effects are mainly due to collisional reorientation of the

* Present address: Philips Research Laboratories, Eindhoven, The Netherlands.

radiating molecules. A second elastic contribution, caused by the rotational phase shift in a collision, is generally much smaller. At not too high densities the pressure broadened Raman lines are well separated from each other and the line shape is lorentzian. In this situation a study of the broadening of the lines with density provides information on the relevant collision processes as a function of the rotational quantum number j ($= j_i$).

Note that the situation for the depolarized Rayleigh line, although also originating from the anisotropic part of the polarizability, is essentially different. The broadening occurs as a result of molecular reorientation only (including also in this case the reorientation in inelastic collisions). Furthermore, all rotational states contribute to the depolarized Rayleigh line, which leads in general to a non-lorentzian line shape[1]).

In previous studies, both experimental[5]) and theoretical[6,7]), it was found that in general the widths of rotational Raman lines decrease with increasing j. This can simply be explained by the fact that for high j both energetically inelastic collisions and reorienting collisions become progressively less probable. Inelastic collisions are less probable at higher j because of the larger energy spacings between the rotational levels. That collisional reorientation becomes more difficult for molecules in higher rotational states is due to the increased gyroscopic stability.

It has been pointed out by Van Kranendonk[6]) that a special case is formed by gases for which the energy spacings between the most populated rotational levels are large with respect to the average thermal energy. Since in such a situation inelastic collisions are infrequent, so-called resonance collisions may be relatively more important. In this type of collision the rotational energy changes of the radiating molecule and its collision partner exactly compensate each other, *i.e.*, there is no energy exchanged between rotational and translational degrees of freedom. While such resonance processes are not detected in studies of rotational relaxation by means of sound absorption experiments[8]), in rotational Raman scattering their effect can indeed be observed. This has recently been indicated in studies on the broadening of HCl Raman lines.[9-11])

The hydrogen isotopes seem well suited to study such resonance collisions[6]).

This has also become apparent from a study on the importance of various multipole interactions for the thermal conductivity of the hydrogen isotopes[12]). The energy level splitting is large and at room temperature only a few rotational levels are populated. Fig. 1 shows schematically the energy level diagram for H_2. For the homonuclear molecule H_2 (and also for D_2) transitions between ortho and para states are forbidden so that the smallest possible collisional jumps on the rotational ladder correspond to $\Delta j = \pm 2$. In HD, on the other hand, collisional transitions with $\Delta j = \pm 1$ are also allowed.

In order to investigate the collisional resonance effects we measured the pressure broadening of the rotational Raman lines in $n H_2$, HD and $n D_2$ at room tempera-

ture (293 K). For H_2 the linewidths have also been measured at various ortho-para compositions. Only the Stokes lines, corresponding to the spectroscopic transitions $\Delta j = j_f - j_i = +2$ were examined in detail. The anti-Stokes lines, which are much weaker, should show an identical behaviour. In H_2 the lines $S_o(0)$ ($j = 0 \rightarrow j = 2$) through $S_o(4)$ ($j = 4 \rightarrow j = 6$) have been observed. In the pure rotational Raman spectrum the S refers to transitions with $\Delta j = +2$ (the subscript o indicates that only the lowest vibrational state is involved). The spectroscopic transitions for the investigated H_2 Raman lines have been indicated in fig. 1. Higher lines were too weak to be detected. In HD and nD_2 the pressure broadening was investigated for the lines $S_o(0)$ through $S_o(4)$ and $S_o(0)$ through $S_o(5)$, respectively. Preliminary results of this study have already been presented[13]).

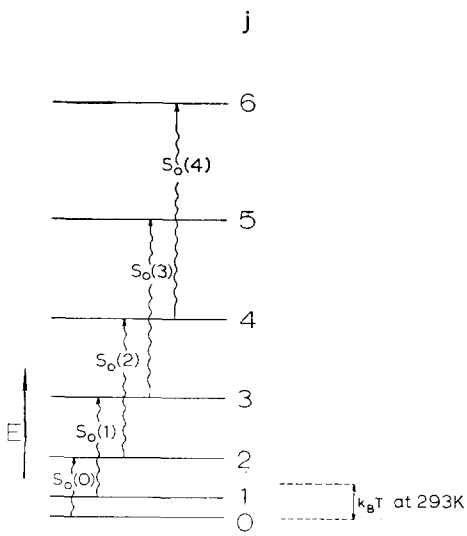

Fig. 1. Rotational energy level diagram for H_2 with Raman transitions.

2. *Experimental.* The experimental arrangement for measuring the rotational Raman lines at room temperature is shown schematically in fig. 2. The beam of an argon ion laser was focussed into a chamber which contained the sample gas at pressures up to 125 atm. The polarization of the light was vertical to the scattering plane. Scattered light was collected at right angles to the source. A small monochromator was utilized to isolate the region of the spectrum containing the individual Raman line of interest. This line was then spectrally analysed with a pressure scanned Fabry–Pérot interferometer and standard photon counting equipment. As the setup is basically identical to the one used for the depolarized Rayleigh scattering experiments[1]), we discuss only the experimental details that are different from those described there.

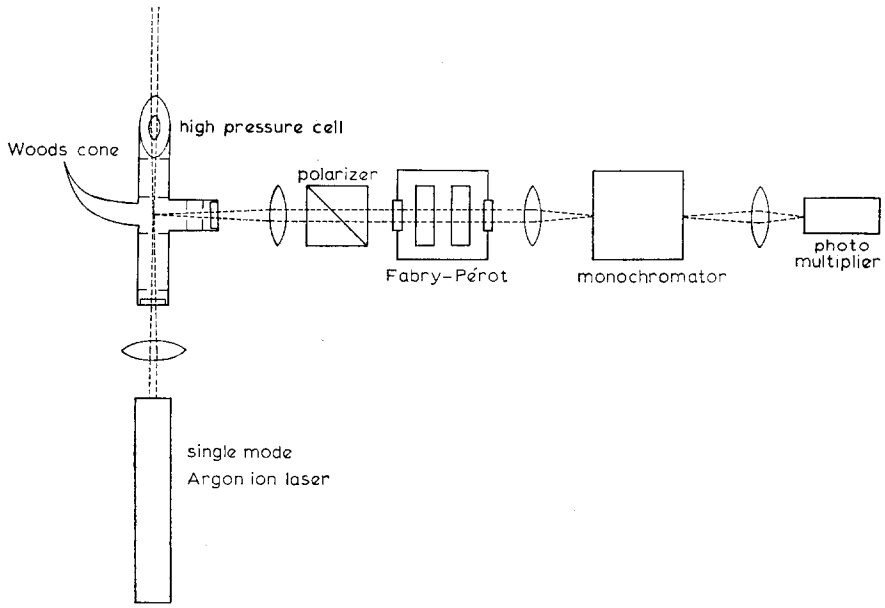

Fig. 2. Schematic diagram of the apparatus.

2.1. Laser. A single (longitudinal) mode argon ion laser (Spectra Physics model 165), operating at the green 5145 Å line, served as a light source. The advantage of the argon laser over the 6328 Å He–Ne laser source, that was used in previous experiments[1,2]), is the considerable gain in signal: (1) the optical power available with the argon laser (600 mW) is about a factor of 10 greater than with the He–Ne laser, (2) the higher frequency of the argon laser line increases the amount of scattered light according to the fourth power of the frequency and (3) the photomultiplier is more sensitive to green light than to red light. In the Raman experiments such a gain in signal proved to be especially useful since it allowed an investigation of several weak lines, that would otherwise not have been possible. A further advantage of the argon laser is that the laser linewidth is negligible, when the laser is operated in a single longitudinal mode.

2.2. Interferometer. The Fabry–Pérot interferometer that was used for the spectral analysis of the rotational Raman lines was equipped with two flat mirrors coated for 98% reflection at 5145 Å. For all experiments a 0.198 cm spacer was used, giving a free spectral range (FSR) of 75.6 GHz. The instrumental profile was determined by scanning the unbroadened laser line. An example of such an instrumental profile, showing the laser line for two consecutive orders of the Fabry–Pérot transmission profile, is given in fig. 3. The overall finesse is about 40. It is seen that the instrumental profile is somewhat asymmetric which is due to

imperfect flatness of the interferometer mirror surfaces. The consequences of this will be discussed later. Another complication is the fact that the instrumental linewidth is slightly wavelength dependent in the spectral range of interest. This is mainly caused by the fact that the reflectance of the interferometer mirrors decreases from 98% at 5145 Å to about 96.5% at 5500 Å. A correction for this effect – in most cases less than 1% – has been applied in the analysis of the experimental data.

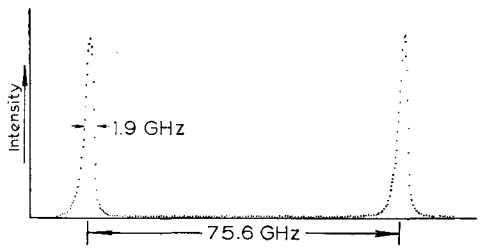

Fig. 3. Typical instrumental profile. Free spectral range (FSR): 75.6 GHz. Instrumental bandwidth: 1.9 GHz. Finesse (*i.e.*, the ratio of free spectral range and instrumental bandwidth): 40.

2.3. Monochromator and polarizer. After transmission by the interferometer the light was focussed onto the entrance slit of a 25 cm Jarrel Ash monochromator (spectral slit width 6 Å or 15 Å), employed to isolate a particular Raman line in the spectrum of the scattered light. This isolation was essential since otherwise a severe overlapping of different orders of the Fabry–Pérot interferometer would have occurred in the spectral analysis. The use of a monochromator for this purpose is very convenient in this type of experiment, since it allows switching from one Raman line to another without realigning the optics. Using interference filters in such a situation is awkward since different lines require different filters.

The very strong polarized Rayleigh–Brillouin triplet was insufficiently rejected by the monochromator. Therefore it was decided to use a Glan–Thompson prism to eliminate the polarized spectrum. Consequently, only the depolarized component of the Raman spectrum was observed in the experiment. This does not affect the interpretation of the results since the pressure broadening of rotational Raman lines is known to be independent of the direction of polarization[14]).

For further details of the setup and the experimental procedure see ref. 1.

2.4. Gas handling. The gases H_2 and D_2 were obtained commercially. Their purity was better than 99%. HD was produced by the action of D_2O on $LiAlH_4$[15]). Its purity could be determined by scanning the entire rotational Raman spectrum and comparing the intensities of H_2 and D_2 lines with those of HD lines (fig. 4).

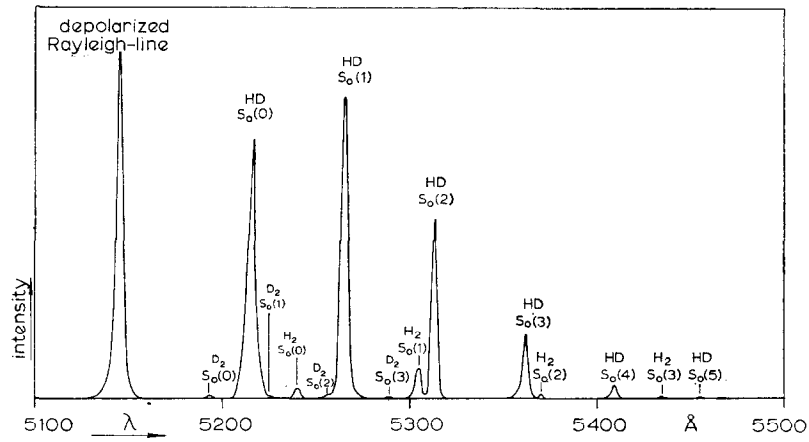

Fig. 4. Analysis of the isotopic purity of HD. The rotational Raman spectrum shows weak H_2 and D_2 lines. The intensity ratio of the various lines indicates that the sample contains 96.5% HD, 3% nH_2 and 0.5% nD_2.

The HD used was found to contain about 3% H_2 and 0.5% D_2. Para H_2 was produced by catalytic conversion of normal H_2 at liquid-hydrogen temperature. At the start of the experiments the para concentration was more than 96%. In the scattering cell, however, the pH_2 slowly converted back into nH_2. The conversion rate was sufficiently slow that measurements could be made as a function of ortho–para composition. For each experiment the ortho–para composition could be determined within 2% by comparing the integrated intensities of odd and even lines.

3. *Calculation of the results.* Examples of experimental interferograms (spectra) of rotational Raman lines are shown in fig. 5. For each of the gases nH_2, HD and nD_2 a typical interferogram is given. The two peaks correspond to consecutive orders of the Fabry–Pérot transmission profile. The measured intensities depend on the particular Raman line investigated. For the most intense lines a peak intensity of a few hundred counts per second was obtained. The weakest lines gave only 3–4 counts per second at the peak.

It is noted that the HD Raman lines are an order of magnitude broader than the nH_2 and nD_2 lines (see fig. 5). An explanation of this effect will be given in section 4.3. In some cases the HD lines were so broad that a fraction of the intensity in the far wings was cut off by the monochromator. A correction for this effect – at the most 3.5% of the total intensity of the line – has been applied. The interferograms were also corrected for the photomultiplier darkcount (typically 0.3 counts per second), which contributed to the spectrum as a flat background.

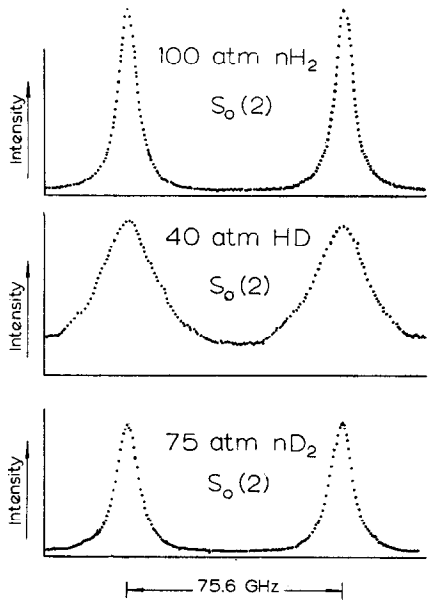

Fig. 5. Examples of Raman line interferograms.

At this stage, an interferogram, described by a function $S(\nu)$ still contains the instrumental contribution. In fact $S(\nu)$ is a convolution of the true Raman line profile $R(\nu)$ with the periodic instrumental function $O(\nu)$:

$$S(\nu) = R(\nu) * O(\nu) = \int_{-\infty}^{+\infty} R(\nu')\, O\,(\nu - \nu')\, \mathrm{d}\nu'. \tag{1}$$

To separate the two contributions a Fourier transform technique is applied. The Fourier transforms of the functions in eq. (1) obey the relation

$$F_S(t) = F_R(t) \cdot F_O(t). \tag{2}$$

$F_R(t)$, the transform of the net Raman line profile is now easily obtained once $F_S(t)$ and $F_O(t)$ have been determined from the experimental quantities $S(\nu)$ and $O(\nu)$.

In a situation where the spectral profiles are fully symmetrical, the calculation of $F_S(t)$ and $F_O(t)$ requires only a cosine transformation. Since, in this case, $O(\nu)$ is slightly asymmetrical, the sine transforms have to be included as well. One has

$$F_S(t) = F_S^+(t) + \mathrm{i}F_S^-(t) \tag{3}$$

and

$$F_O(t) = F_O^+(t) + iF_O^-(t), \tag{4}$$

where F^+ and F^- denote the cosine and sine transforms, respectively. They are calculated from the experimental interferograms as described in ref. 1. The normalization is chosen such that $F_S(0) = F_O(0) = 1$. $F_R(t)$ is now given by

$$F_R(t) = \frac{F_S(t)}{F_O(t)} = \frac{F_S^+(t)\,F_O^+(t) + F_S^-(t)\,F_O^-(t)}{[F_O^+(t)]^2 + [F_O^-(t)]^2}$$

$$+ i\frac{F_S^-(t)\,F_O^+(t) - F_S^+(t)\,F_O^-(t)}{[F_O^+(t)]^2 + [F_O^-(t)]^2}. \tag{5}$$

It was always found that the imaginary part of $F_R(t)$ was zero. The Raman line profiles are thus symmetrical, as should be the case. $F_R(t)$ is therefore calculated as the first term in eq. (5).

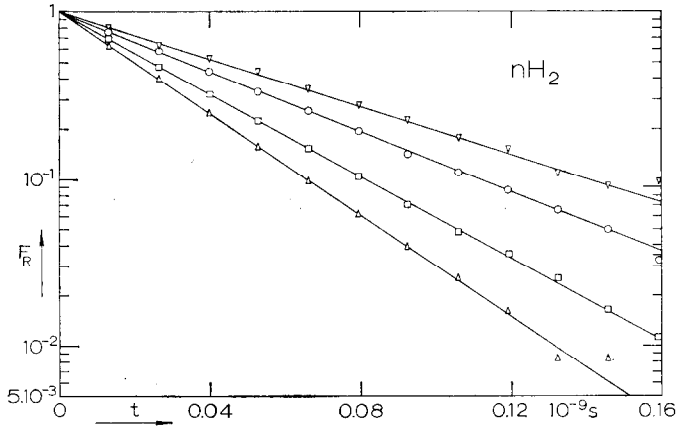

Fig. 6. F_R as a function of t for some rotational Raman lines of $n\mathrm{H}_2$. □ $S_0(0)$ 124.5 atm, △ $S_0(1)$ 124.5 atm, ○ $S_0(2)$ 100 atm, ▽ $S_0(4)$ 124.5 atm.

Typical results for F_R as a function of time for some Raman line profiles of the gases $n\mathrm{H}_2$, HD and $n\mathrm{D}_2$ are given in figs. 6–8. The semilogarithmic plots show a linear behaviour in all cases. $F_R(t)$ has thus a simple exponential form and can be written as

$$F_R(t) = e^{-2\pi\Delta\nu_{\frac{1}{2}}t}, \tag{6}$$

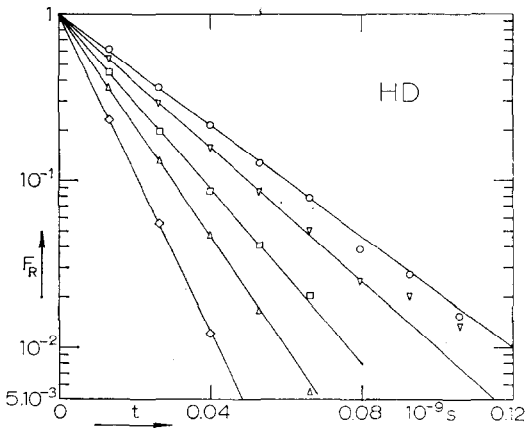

Fig. 7. F_R as a function of t for some rotational Raman lines of HD. □ $S_0(0)$ 25 atm, ◇ $S_0(1)$ 50 atm, △ $S_0(2)$ 40 atm, ○ $S_0(3)$ 25 atm, ▽ $S_0(4)$ 40 atm.

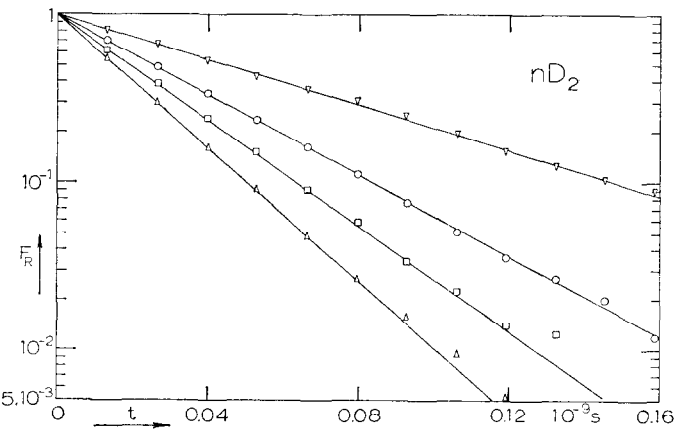

Fig. 8. F_R as a function of t for some rotational Raman lines of nD_2. △ $S_0(0)$ 100 atm, □ $S_0(1)$ 96 atm, ○ $S_0(3)$ 96 atm, ▽ $S_0(5)$ 96 atm.

where $\Delta\nu_{\frac{1}{2}}$ is the half-width (half the width at half intensity) of the associated lorentzian line profile:

$$R(\nu) = \frac{I_0}{\pi} \frac{\Delta\nu_{\frac{1}{2}}}{\nu^2 + \Delta\nu_{\frac{1}{2}}^2}. \tag{7}$$

I_0 is the total integrated intensity of the Raman line and the central frequency of the line has been taken zero.

The half-width $\Delta\nu_{\frac{1}{2}}$ is the characteristic parameter for the broadening of the Raman lines. It is easily determined from the plots of F_R *versus* t.

4. *Experimental results and discussion.* 4.1. HD, nH$_2$ and nD$_2$. Results are presented for the pressure broadened rotational Raman lines of HD, normal H$_2$ and normal D$_2$ at 293 K. Normal H$_2$ consists of $\frac{3}{4}$ ortho (odd j) and $\frac{1}{4}$ para (even j) and normal D$_2$ of $\frac{2}{3}$ ortho (even j) and $\frac{1}{3}$ para (odd j).

HD is discussed first, as the HD results follow the usual trend and have a simple explanation. The HD Raman lines have been investigated in the pressure range of 25–75 atm. The half-widths $\Delta\nu_{\frac{1}{2}}$ of the lines $S_0(0)$ through $S_0(4)$ are given in fig. 9 as a function of the density ϱ. $\Delta\nu_{\frac{1}{2}}$ is found to be linear in the density, as expected*. Broadening coefficients $\Delta\nu_{\frac{1}{2}}/\varrho$ have been obtained from the slopes and are given in table I and fig. 10. It is seen that the broadening coefficients decrease smoothly with j. Such a monotonic decrease has also been found in pressure broadening studies of rotational Raman lines of larger molecules[5]). As pointed out in section 1 such a behaviour is due to the fact that both inelastic and reorientation cross sections decrease with increasing j.

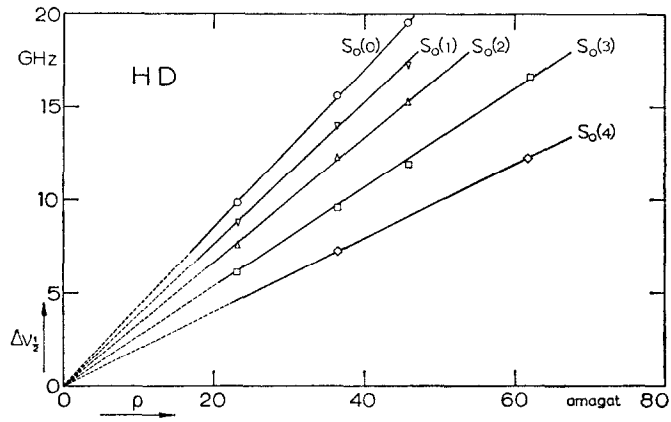

Fig. 9. $\Delta\nu_{\frac{1}{2}}$ as a function of ϱ for the rotational Raman lines of HD.

The Raman lines of nH$_2$ were investigated in the pressure range of 75–125 atm. The results for $\Delta\nu_{\frac{1}{2}}$ *versus* ϱ are given in fig. 11. Values for $\Delta\nu_{\frac{1}{2}}/\varrho$ are presented in table I and fig. 12. Previously obtained results for the broadening of the $S_0(0)$ and $S_0(1)$ lines are in excellent agreement with the present results.

* The translational motion of the molecules gives rise to a contribution with a different density dependence. For the hydrogen isotopes this effect has been shown to be unimportant at pressures above 25 atm[16–18]).

TABLE I

Broadening coefficients of rotational Raman lines

	$\Delta\nu_{\frac{1}{2}}/\varrho$ in GHz/amagat			
	HD	nH$_2$		nD$_2$
		this exp.	literature	
$S_0(0)$	0.43 ± 0.01	0.042 ± 0.001	0.042 ± 0.001[a]	0.084 ± 0.001
$S_0(1)$	0.38 ± 0.01	0.052 ± 0.001	0.053 ± 0.001[a]	0.067 ± 0.001
			0.054 ± 0.002[b]	
$S_0(2)$	0.33 ± 0.01	0.037 ± 0.001	–	0.062 ± 0.001
$S_0(3)$	0.27 ± 0.01	0.038 ± 0.001	–	0.051 ± 0.001
$S_0(4)$	0.20 ± 0.01	0.023 ± 0.001	–	0.043 ± 0.001
$S_0(5)$	–	–	–	0.028 ± 0.001

A density of 1 amagat corresponds approximately to 2.687×10^{19} molecules/cm^3.
[a] Ref. 17; [b] ref. 18.

The broadening coefficients $\Delta\nu_{\frac{1}{2}}/\varrho$ for nH$_2$ show a behaviour that deviates markedly from the pattern found for HD. Instead of a regular decrease of the broadening with j, a distinct alternation is observed, the odd lines being relatively broader than the even ones.

This alternation of the broadening with j can be explained by the fact that resonance collisions play an important role in the broadening. In nH$_2$ at room temperature about $\frac{2}{3}$ of the molecules are in the $j = 1$ state (see table II). Molecules

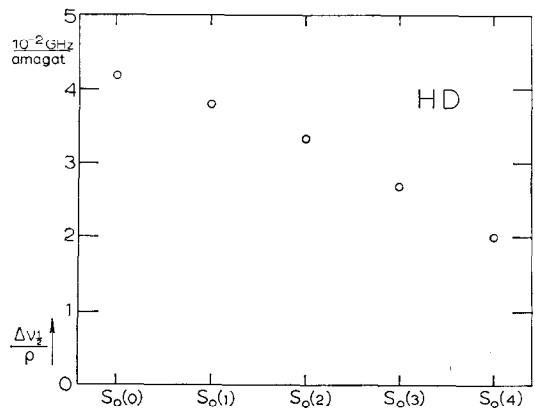

Fig. 10. $\Delta\nu_{\frac{1}{2}}/\varrho$ for the rotational Raman lines of HD.

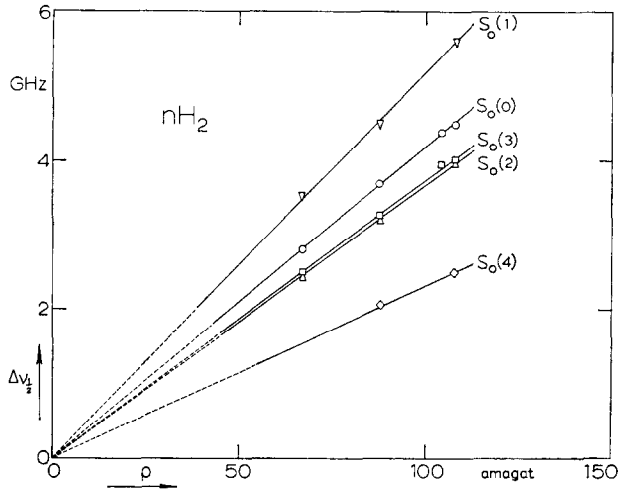

Fig. 11. $\Delta\nu_{\frac{1}{2}}$ as a function of ϱ for the rotational Raman lines of nH_2.

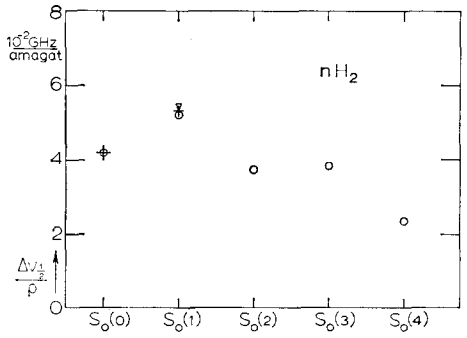

Fig. 12. $\Delta\nu_{\frac{1}{2}}/\varrho$ for the rotational Raman lines of nH_2. ○ present results; + Cooper *et al.*[17]); ▽ Gupta and May[18]).

in the $j = 3$ state are the only ones that can undergo resonance collisions with the abundant $j = 1$ molecules. If these resonance collisions are important a significantly shorter life time for molecules in the $j = 3$ state results. This in turn causes extra broadening for the spectroscopic lines involving this state, *viz.* $S_0(1)$ and $S_0(3)$.

The results for the Raman lines of nD_2 (see figs. 13 and 14 and table I) show a similar alternation in the broadening coefficients, although not as pronounced as in nH_2. The effect is here just opposite to that for nH_2, which is consistent with the reasoning above, since in nD_2 the even levels are more densely populated than the odd ones.

TABLE II

Fractional population of H_2 rotational levels at 293 K

j	Ortho H_2	Normal H_2 ($\frac{3}{4}oH_2 + \frac{1}{4}pH_2$)	Para H_2
0	–	0.132	0.525
1	0.884	0.662	–
2	–	0.115	0.460
3	0.115	0.086	–
4	–	0.004	0.015
5	0.001	0.001	–
6	–	0.000	0.000

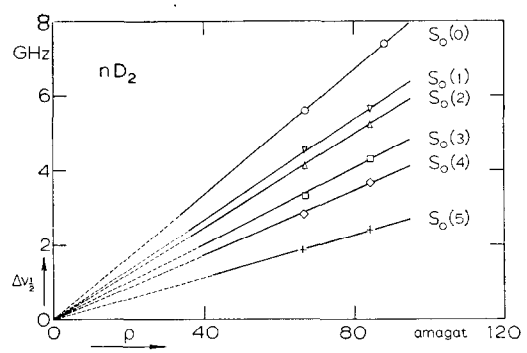

Fig. 13. $\Delta\nu_{\frac{1}{2}}$ as a function of ϱ for the rotational Raman lines of nD_2.

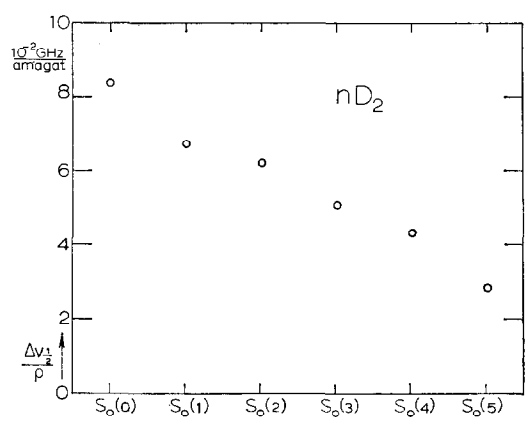

Fig. 14. $\Delta\nu_{\frac{1}{2}}/\varrho$ for the rotational Raman lines of nD_2.

4.2. Mixtures of oH_2–pH_2. To further test the hypothesis of the importance of resonance collisions, we decided to vary for H_2 the relative populations of the odd and even rotational states by making measurements for different mixtures of ortho and para hydrogen (*cf.* table II). This could easily be accomplished by performing measurements on a sample of pure para hydrogen at 124.5 atm, which was allowed to convert slowly to normal hydrogen. The lines $S_0(0)$ to $S_0(4)$ were investigated at para concentrations ranging from about 0.96 down to 0.46. The resulting half-widths for the various lines are plotted *versus* concentration pH_2 in fig. 15. The points for $x_{pH_2} = 0.25$ correspond to the nH_2 results of the preceding section. It is seen that the linewidths for all lines vary linearly with concentration as should be expected at a density where only binary collisions are important.

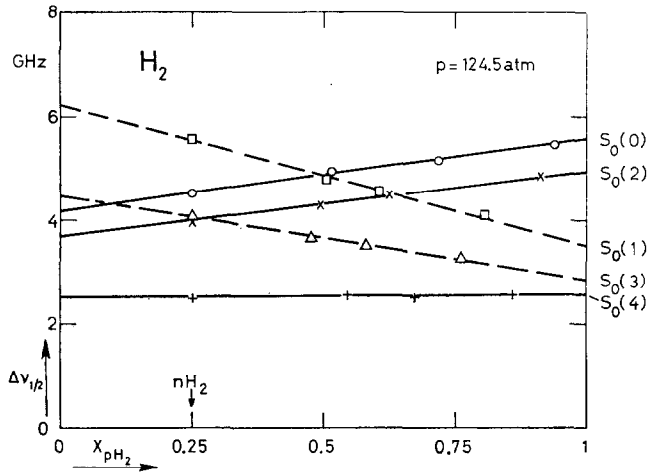

Fig. 15. The linewidths of the rotational Raman lines of H_2 as a function of ortho–para composition.

The different slopes for the various lines indicate very clearly the important contribution of resonance collisions to the linewidths. At high para concentration one expects resonance effects to be important in collisions between molecules with even j. This explains the increase of the linewidth with concentration for the $S_0(0)$ and $S_0(2)$ lines (solid lines in fig. 15). For the $S_0(1)$ and $S_0(3)$ lines (dotted lines) the situation is just reversed, resonance being important at low para concentration. This results in a decrease of the corresponding linewidths as a function of para concentration, further corroborating the importance of resonance collisions.

Of course the linewidths also contain contributions from other types of inelastic collisions and also from energetically elastic collisions. In connection with the observed variation of the linewidths with concentration it should be pointed out

that so-called quasi-resonance collisions, *i.e.*, collisions in which the rotational energy change of one molecule is only partly compensated by the rotational energy change of its collision partner, may give an important contribution to the linewidths. An example of a quasi-resonance collision is, *e.g.*, $j = 1 \rightarrow j = 3$ combined with $j = 2 \rightarrow j = 0$ of the collision partner. Such a collision may energetically be more favourable than a collision, in which only one of the colliding molecules changes its rotational state. Since the total rotational energy change in a quasi-resonance collision is smallest when both the upper and lower j states involved in the collisional transitions differ by only one unit, it is expected that such collisions mainly occur between ortho molecules and para collision partners. This gives rise to a contribution to the linewidths with a concentration dependence just opposite to that of the exact resonance collisions.

A direct separation of the various contributions on the basis of the experimental results alone is not possible. From a comparison of the extrapolated linewidth values for pure ortho and para, however, it can be concluded that the contribution of (exact) resonance collisions for some of the lines exceeds 40% of the total linewidth. The total contribution of resonance and quasi-resonance collisions is probably considerably higher. It can therefore be concluded that the angle-dependent part of the H_2 potential must contain an important term that allows for simultaneous transitions of collision partners, *e.g.*, the quadrupole–quadrupole interaction. A theoretical description for the broadening of the H_2 rotational Raman lines, based on such a quadrupole–quadrupole interaction, has been given by Van Kranendonk[6]) and Moraal[23]). In section 5 we will compare our results with this theory.

4.3. Effective cross sections. It is often useful to express the experimental results in terms of effective cross sections, especially so since these are a better measure in the comparison of the results. Therefore we use the broadening coefficients and linewidths obtained in the preceding sections to calculate effective cross sections $\mathcal{C}_{RR}$ with the relation

$$2\pi \Delta\nu_{\frac{1}{2}} = n\langle v\rangle_0 \, \mathcal{C}_{RR}. \tag{8}$$

n is the density number and $\langle v\rangle_0$ the average relative velocity, given by

$$\langle v\rangle_0 = (8k_B T/\pi\mu)^{\frac{1}{2}} \tag{9}$$

with μ the reduced mass, k_B Boltzmann's constant and T the absolute temperature. For H_2 at 293 K, $\langle v\rangle_0$ is 2485 m/s.

Values for $\mathcal{C}_{RR}$ for the rotational Raman lines of HD, nH$_2$ and nD$_2$ are presented in table III. A remarkable fact is that the effective cross sections for HD are an order of magnitude larger than those for nH$_2$ and nD$_2$. The cause of this

TABLE III

Effective Raman line cross sections

	$\mathcal{C}_{RR}$ in Å^2		
	HD	nH$_2$	nD$_2$
$S_0(0)$	4.9 ± 0.1	0.40 ± 0.01	1.12 ± 0.01
$S_0(1)$	4.4 ± 0.1	0.49 ± 0.01	0.89 ± 0.01
$S_0(2)$	3.8 ± 0.1	0.35 ± 0.01	0.83 ± 0.01
$S_0(3)$	3.1 ± 0.1	0.36 ± 0.01	0.68 ± 0.01
$S_0(4)$	2.3 ± 0.1	0.22 ± 0.01	0.57 ± 0.01
$S_0(5)$	–	–	0.37 ± 0.01

lies in the asymmetric mass distribution in the HD molecule. This so-called loaded sphere character gives rise to a large P_1 term in the intermolecular potential. Such a P_1-type interaction leads to large inelastic collisional cross sections but does not allow simultaneous transitions of collision partners. The nonspherical part of the intermolecular potential for the homonuclear molecules H_2 and D_2 is much smaller as is also known from, *e.g.*, sound absorption experiments[19]).

Using eq. (8) it is also possible to determine the effective cross sections $\mathcal{C}_{RR}$ for the H_2 Raman lines in the limit of pure oH$_2$ and pure pH$_2$ from the extrapolated values of $\Delta\nu_{\frac{1}{2}}$ (fig. 15). The results are given in table IV.

TABLE IV

Effective Raman line cross sections in the limits of pure oH$_2$ and pH$_2$

	$\mathcal{C}_{RR}$ in Å^2	
	oH$_2$	pH$_2$
$S_0(0)$	0.36 ± 0.01	0.49 ± 0.01
$S_0(1)$	0.54 ± 0.01	0.31 ± 0.01
$S_0(2)$	0.32 ± 0.01	0.43 ± 0.01
$S_0(3)$	0.39 ± 0.01	0.25 ± 0.01
$S_0(4)$	0.22 ± 0.01	0.23 ± 0.01

5. *Comparison with theory.* In order to understand the interpretation of the preceding section more quantitatively, the Raman line cross sections have been calculated using the impact theory of Fiutak and Van Kranendonk[20]). In particular the calculation of Van Kranendonk[6]) is followed which uses a classical path description (straight-line trajectories) for the translational states and neglects the

spread in the velocities. For H_2 it assumes that the dominant term in the angle-dependent part of the intermolecular interaction is quadrupole–quadrupole. Other multipoles as well as induced intermolecular forces are neglected. The calculations have been carried out by Van Kranendonk for normal H_2 and we have extended these to obtain the Raman line cross sections for ortho and para H_2. This is simply accomplished by restricting the rotational averages over the perturbers to either even or odd parity. These calculations, which have been carried out for the lines $S_0(0)$ through $S_0(4)$, are presented in detail in the appendix.

The results of these calculations for the various Raman lines are collected in table V. The contributions from different types of collisions, *viz.* energetically elastic (reorientation), exact resonance, quasi-resonance and inelastic nonresonance, are listed separately. Inelastic nonresonance refers to collisions that are inelastic in only one of the colliding molecules, *i.e.*, either the radiating molecule (Δj_i or $\Delta j_f \neq 0$) or the perturber ($\Delta j_a \neq 0$). It can be seen from table V that for all lines a large fraction of the total broadening cross section is due to resonance and quasi-resonance contributions. The theoretical cross sections for the $S_0(1)$

TABLE V

Effective Raman line cross sections for $\tau = d/v = 0.96 \times 10^{-13}$ s

Cross sections in the limit of pure oH$_2$ (in Å^2)

	Elastic	Inelastic				$\mathfrak{S}_{RR}$	
		res.	quasi-res.	nonres. Δj_i or $\Delta j_f \neq 0$	nonres. $\Delta j_a \neq 0$	Total calc.	Exp.
$S_0(0)$	0.205	–	0.208	0.106	0.000	0.52	0.36
$S_0(1)$	0.248	0.287	0.001	0.000	0.000	0.54	0.54
$S_0(2)$	0.099	–	0.401	0.017	0.000	0.52	0.32
$S_0(3)$	0.056	0.285	0.003	0.000	0.000	0.34	0.39
$S_0(4)$	0.037	–	0.256	0.000	0.000	0.29	0.22

Cross sections in the limit of pure pH$_2$ (in Å^2)

	Elastic	Inelastic				$\mathfrak{S}_{RR}$	
		res.	quasi-res.	nonres. Δj_i or $\Delta j_f \neq 0$	nonres. $\Delta j_a \neq 0$	Total calc.	Exp.
$S_0(0)$	0.072	0.371	0.002	0.037	0.040	0.52	0.49
$S_0(1)$	0.087	–	0.353	0.000	0.049	0.49	0.31
$S_0(2)$	0.034	0.325	0.005	0.006	0.019	0.39	0.43
$S_0(3)$	0.020	–	0.375	0.000	0.011	0.41	0.25
$S_0(4)$	0.013	0.129	0.004	0.000	0.007	0.15	0.23

and $S_0(3)$ Raman lines are compared with the experimental results in fig. 16. In fig. 17 the same is done for the $S_0(0)$, $S_0(2)$ and $S_0(4)$ lines. All calculated cross sections are linear in the para concentration. The distinct alternation in the slopes for the even and odd Raman lines, which is observed experimentally, is not reproduced by the theoretical calculations. This has to be attributed to an underestimation of the resonance collisions in the theory.

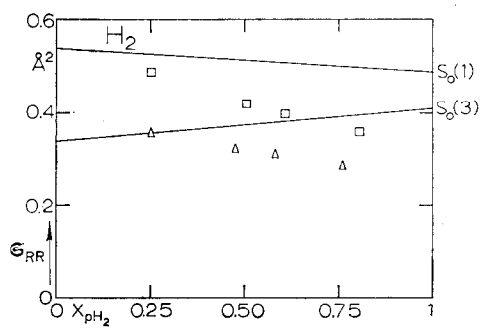

Fig. 16. Comparison between theory and experiment for the $S_0(1)$ and $S_0(3)$ Raman lines. □ $S_0(1)$, △ $S_0(3)$ experimental points; ——— theory with $\tau = d/v = 0.96 \times 10^{-13}$ s.

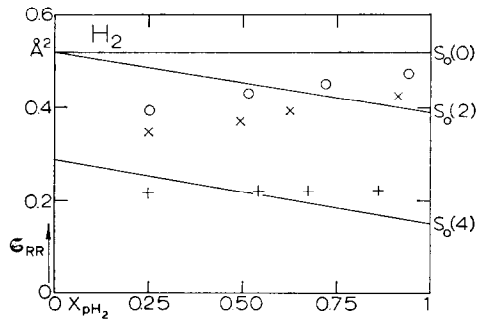

Fig. 17. Comparison between theory and experiment for the $S_0(0)$, $S_0(2)$ and $S_0(4)$ Raman lines. ○ $S_0(0)$, × $S_0(2)$, + $S_0(4)$ experimental points; ——— theory with $\tau = d/v = 0.96 \times 10^{-13}$ s.

In Van Kranendonk's treatment the probability of a collision with an overall rotational energy change of $\hbar\omega$ is proportional to a resonance factor $g_0(\omega\tau)$, where τ measures the duration of the collision. This resonance factor has for the quadrupole–quadrupole interaction the form shown in fig. 18. For exact resonance collisions one has $\omega = 0$ and $g_0(0) = 1$, independent of τ. For other inelastic collision processes, however, the value of $g_0(\omega\tau)$ depends on τ. Thus varying τ changes the efficiency of the inelastic collisions. Van Kranendonk approximated τ for impact parameters larger than the Lennard-Jones diameter d by $\tau = d/v$, with

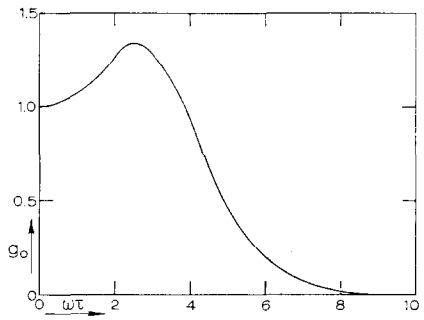

Fig. 18. The resonance factor $g_0(\omega\tau)$ for the quadrupole–quadrupole interaction (reproduced from ref. 6).

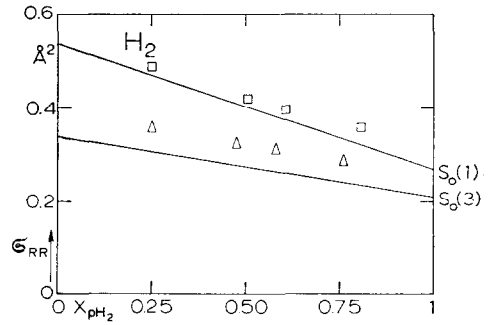

Fig. 19. Comparison between theory and experiment for the $S_0(1)$ and $S_0(3)$ Raman lines. □ $S_0(1)$, △ $S_0(3)$ experimental points; ——— theory with $\tau = 1.18 \times 10^{-13}$ s.

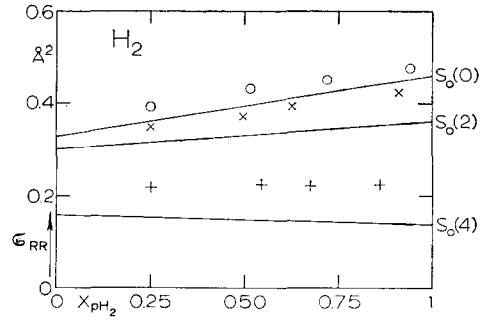

Fig. 20. Comparison between theory and experiment for the $S_0(0)$, $S_0(2)$ and $S_0(4)$ Raman lines. ○ $S_0(0)$, × $S_0(2)$, + $S_0(4)$ experimental points; ——— theory with $\tau = 1.18 \times 10^{-13}$ s.

the relative velocity $v = (3k_BT/\mu)^{\frac{1}{2}}$ (note that v has the same value for all collisions). This choice leads to poor agreement with experiment, as can be seen from figs. 16 and 17. It is found, however, that a slightly larger value for τ (by about 20%) changes the slopes of the lines drastically (see figs. 19 and 20 and table VI). This increase in τ, which is not unreasonable under the approximations, gives much better agreement with the experiment. As can be seen by comparing tables V and VI, the better agreement results from a suppression of the contributions from quasi-resonance and nonresonance collisions.

TABLE VI

Effective Raman line cross sections for $\tau = 1.18 \times 10^{-12}$ s

Cross sections in the limit of pure oH$_2$ (in Å^2)

	Elastic	Inelastic				$\mathfrak{S}_{RR}$	
		res.	quasi-res.	nonres.	nonres.	Total	Exp.
				Δj_i or $\Delta j_f \neq 0$	$\Delta j_a \neq 0$	calc.	
$S_0(0)$	0.205	–	0.103	0.021	0.000	0.33	0.36
$S_0(1)$	0.248	0.287	0.000	0.000	0.000	0.54	0.54
$S_0(2)$	0.099	–	0.199	0.003	0.000	0.30	0.32
$S_0(3)$	0.056	0.285	0.000	0.000	0.000	0.34	0.39
$S_0(4)$	0.037	–	0.127	0.000	0.000	0.16	0.22

Cross sections in the limit of pure pH$_2$ (in Å^2)

	Elastic	Inelastic				$\mathfrak{S}_{RR}$	
		res.	quasi-res.	nonres.	nonres.	Total	Exp.
				Δj_i or $\Delta j_f \neq 0$	$\Delta j_a \neq 0$	calc.	
$S_0(0)$	0.072	0.371	0.000	0.007	0.008	0.46	0.49
$S_0(1)$	0.087	–	0.176	0.000	0.009	0.27	0.31
$S_0(2)$	0.034	0.325	0.000	0.001	0.004	0.36	0.43
$S_0(3)$	0.020	–	0.186	0.000	0.002	0.21	0.25
$S_0(4)$	0.013	0.129	0.000	0.000	0.001	0.14	0.23

Although the agreement between theory and experiment may seem satisfactory, the very fact that the final results of the calculation are so sensitive to the choice of τ, indicates that a re-evaluation of the approximations in this theory is required.

In these calculations the contributions from inelastic nonresonance collisions in ortho H_2, *i.e.*, $j = 1 \rightarrow 3$ or $j = 3 \rightarrow 1$, are effectively zero (see table V and VI). However, a value of 0.073 Å^2 is found for the cross section for rotational relaxation in ortho H_2[21]), which results almost exclusively from the $1 \rightleftarrows 3$ transitions.

An explanation of this discrepancy is that interactions other than quadrupole–quadrupole may also be important. In fact theoretical studies of rotational relaxation usually assume a short-range P_2-type interaction to be the dominant one for nonresonance collisions, while the (long-range) quadrupole–quadrupole term is neglected. It seems reasonable to assume that such contributions from the short-range interactions cannot be ignored in the H_2 Raman line broadening.

Similar conclusions may be drawn from experiments on the pressure broadening of H_2 rotational Raman lines by noble gases[17,18,22]). Although in the H_2-noble-gas interaction, the quadrupole–quadrupole term is obviously absent, the broadening of the H_2 Raman lines by noble gases is found to be only a factor 2 smaller than the self-broadening. This strongly suggests that the self-broadening cannot be attributed to quadrupole–quadrupole alone[17]).

Recently theoretical calculations of the self-broadening of the rotational Raman lines in H_2 based on a distorted wave Born approximation have been performed[23]). A P_2-type of interaction is used in addition to the quadrupole–quadrupole term. Satisfactory agreement with the experimental results presented here is reported.

APPENDIX

In this appendix the formulae from which the cross sections in tables V and VI were calculated are summarized. The details can be found in Van Kranendonk's paper[6]) and only a brief outline is given here.

The half-width (at half intensity) for the $S_0(j)$ Raman lines is given in eq. (44) of ref. 6 by

$$\Delta\nu_{\frac{1}{2}} = \frac{nv\mathfrak{S}^J_{RR}}{2\pi} = \frac{28Q^4L(T)\,n}{75\hbar^2vd^6}\,\bar{S}(j, j+2, 2). \tag{A.1}$$

In eq. (A.1), Q is the quadrupole moment, n the number density, d the molecular diameter and $L(T)$ a normalization function given by

$$L(T) = \sum_{j_a=0}^{\infty} p(j_a)\,C(j_a 2 j_a; 000)^2. \tag{A.2}$$

$p(j_a)$ is the Boltzmann weight and $C(...)$ is a Clebsch–Gordan coefficient.

The dimensionless function $\bar{S}(j_i, j_f, 2)$ is the fundamental quantity which determines the linewidths for anisotropic Raman transitions between states j_i and j_f. For the $S_0(j)$ lines one has for the initial state $j_i = j$ and for the final state $j_f = j + 2$. Calculations of $\bar{S}$ can be accomplished analytically by treating the collision process as a simple straight-line trajectory and neglecting molecular

reorientations during the time of collisions. Explicitly for S branch Raman lines $\bar{S}$ is given by [eqs. (33) and (41) of ref. 6]

$$\bar{S}(j_i, j_f, 2) = D(j_i, j_f, 2)\, g(0) + C(j_i, 2, j_i + 2; 000)^2\, g(\omega_{j_i, j_i+2}\tau) + C(j_i, 2, j_i - 2; 000)^2\, g(\omega_{j_i, j_i-2}\tau) + (\mathrm{i} \to \mathrm{f}), \tag{A.3}$$

where

$$D(j, j+2; 2) = \frac{6(4j^2 + 12j - 3)}{(2j-1)(2j+3)^2(2j+7)}. \tag{A.4}$$

This factor and the Clebsch–Gordan coefficients arise from the traces over the internal states. The rotational energy change for a collisional transition from $j \to j'$ is given by $\hbar\omega_{jj'}$. The quantity τ measures the duration of a collision and is approximated by

$$\tau = d/v \qquad \text{with} \qquad v = (3k_B T/\mu)^{\frac{1}{2}}. \tag{A.5}$$

The resonance factors,

$$g(\omega\tau) = g_0(\omega\tau) + g_+(\omega\tau) + g_-(\omega\tau) \tag{A.6}$$

arise from the time integration over the collision process for impact parameter $b > d$. Under the assumption that the intermolecular potential is quadrupole–quadrupole, the function $g_0(\omega\tau)$ is given explicitly in terms of modified Bessel functions $K_\mu(\omega\tau)$ by

$$g_0(\omega\tau) = (35/2) \sum_{\mu=-4}^{4} [(4+\mu)!\,(4-\mu)!\,2]^{-1}\, (\omega\tau)^8\, K_\mu^2(\omega\tau). \tag{A.7}$$

This function has been plotted in fig. 18. The terms $g_\pm(\omega\tau)$ are given in terms of $g_0(\omega\tau)$,

$$g_\pm(\omega\tau) = L(T)^{-1} \sum_{j_a} p(j_a)\, C(j_a, 2, j_a \pm 2; 000)^2\, g_0(\omega_{j_a, j_a \pm 2}\tau + \omega\tau), \tag{A.8}$$

where the sum j_a is over the colliding partner. In extending these calculations to ortho and para species, the average over the colliding partner in eqs. (A.2) and (A.8) was restricted to either odd j_a (ortho colliding partner) or even j_a (para colliding partner). It is clear that an ortho (para) radiating molecule in a bath of ortho (para) perturbers can undergo a resonance collision, whereas in the opposite

limit, ortho (para) in a bath of para (ortho) perturbers, resonance collisions cannot occur. For the $S_0(j)$ lines, cross sections can be defined by

$$\mathfrak{S}^j_{RR}\,(\text{ortho}) = \frac{56\pi\, Q^4 L^{\text{ortho}}(T)}{75\hbar^2 v^2 d^6}\, \bar{S}^{\text{ortho}}(j, j+2, 2) \tag{A.9}$$

and

$$\mathfrak{S}^j_{RR}\,(\text{para}) = \frac{56\pi\, Q^4 L^{\text{para}}(T)}{75\hbar^2 v^2 d^6}\, \bar{S}^{\text{para}}(j, j+2, 2), \tag{A.10}$$

where the superscripts ortho and para refer to the appropriate restrictions on the j_a sums over the colliding partner.

In order to calculate the cross sections for the various collisional processes, the $\bar{S}(j, j+2, 2)$ term in eq. (A.3) was broken up into several parts. The various columns in tables V and VI contain different contributions to $\mathfrak{S}^j_{RR}$ corresponding to the following conditions on eq. (A.3):

1) Elastic collisions which require no collisional changes in j_i, j_f or j_a, hence,

$$\bar{S}(j_i, j_f, 2)_{el} \equiv D(j_i, j_f, 2)\, g_0(0). \tag{A.11}$$

2) The contributions from resonance collisions can be found by imposing the condition on the collisions that $\Delta j_i = -\Delta j_a$ with $j_i' = j_a$ or $\Delta j_f = -\Delta j_a$ with $j_f' = j_a$.

3) The contributions from quasi-resonance collisions are obtained from eq. (A.3) by requiring that $\Delta j_i = -\Delta j_a$ with $j_i' \neq j_a$ or $\Delta j_f = -\Delta j_a$ with $j_f' \neq j_a$.

4) Nonresonance collisions require that either the radiating molecule or the collision partner, but not both, undergo a collisional transition. These conditions are that a) Δj_i or $\Delta j_f \neq 0$ with $\Delta j_a = 0$, or b) Δj_i and $\Delta j_f = 0$ with $\Delta j_a \neq 0$.

The resulting $\bar{S}$ matrix terms have been used with eqs. (A.9) and (A.10) to obtain the various contributions to the cross sections, in tables V and VI. The five columns labelled elastic, resonance, quasi-resonance, nonresonance (Δj_i or $\Delta j_f \neq 0$) and nonresonance ($\Delta j_a \neq 0$) correspond to procedures 1), 2), 3), 4a) and 4b), respectively. It should be pointed out that the organization described here does not follow that used by Van Kranendonk.

Finally it is possible to calculate the $S_0(j)$ lines for normal H_2 by use of,

$$\mathfrak{S}^j_{RR}\,(\text{normal}) = 0.75\mathfrak{S}^j_{RR}\,(\text{ortho}) + 0.25\mathfrak{S}^j_{RR}\,(\text{para}) \tag{A.12}$$

and the cross sections thus obtained agree with those calculated by Van Kranendonk for normal H_2.

Acknowledgements. The authors would like to thank Drs. M. de Groot for his valuable assistance during this research and Professor J.J.M. Beenakker for his interest and helpful discussions.

This work is part of the research program of the "Stichting voor Fundamenteel Onderzoek der Materie (F.O.M.)" and has been made possible by financial support from the "Nederlandse Organisatie voor Zuiver Wetenschappelijk Onderzoek (Z.W.O.)".

REFERENCES

1) Keijser, R.A.J., Van den Hout, K.D., De Groot, M. and Knaap, H.F.P., Physica **75** (1974) 515 (Commun. Kamerlingh Onnes Lab., Leiden No. 408*a*).
2) Keijser, R.A.J., Van den Hout, K.D. and Knaap, H.F.P., Physica **76** (1974) 577 (Commun. Kamerlingh Onnes Lab., Leiden No. 408*b*).
3) Gordon, R.G., J. chem. Phys. **44** (1966) 3083.
4) Shafer, R. and Gordon, R.G., J. chem. Phys. **58** (1973) 5422.
5) Jammu, K.S., St.John, G.E. and Welsh, H.L., Can. J. Phys. **44** (1966) 797.
6) Van Kranendonk, J., Can. J. Phys. **41** (1963) 433.
7) Gray, C.G. and Van Kranendonk, J., Can. J. Phys. **44** (1966) 2411.
8) Sluijter, C.G., Knaap, H.F.P. and Beenakker, J.J.M., Physica **30** (1964) 745 (Commun. Kamerlingh Onnes Lab., Leiden No. 337*c*).
Jonkman, R.M., Prangsma, G.J., Keijser, R.A.J., Aziz, R.A. and Beenakker, J.J.M., Physica **38** (1968) 451 (Commun. Kamerlingh Onnes Lab., Leiden No. 365*b*).
9) Rich, N.H. and Welsh, H.L., Chem. Phys. Letters **11** (1971) 292.
10) Fabre, D., Widenlocher, G. and Vu, H., Optics Commun. **4** (1972) 421.
11) Gray, C.G., Chem. Phys. Letters **8** (1971) 527.
12) Nyeland, C., Mason, E.A. and Monchick, L., J. chem. Phys. **56** (1972) 6180.
13) Keijser, R.A.J., Lombardi, J.R., Van den Hout, K.D., De Groot, M., Sanctuary, B.C. and Knaap, H.F.P., Phys. Letters **45A** (1973) 3.
14) Gupta, B.K., Hess, S. and May, A.D., Can. J. Phys. **50** (1972) 778.
15) Fookson, A., Pomerantz, P. and Rich, E.H., J. Res. Natl. Bur. Std. **47** (1951) 31.
16) Cooper, V.G., May, A.D., Hara, E.H. and Knaap, H.F.P., Can. J. Phys. **46** (1968) 2019.
17) Cooper, V.G., May, A.D. and Gupta, B.K., Can. J. Phys. **48** (1970) 725.
18) Gupta, B.K. and May, A.D., Can. J. Phys. **50** (1972) 1747.
19) Prangsma, G.J., Heemskerk, J.P.J., Knaap, H.F.P. and Beenakker, J.J.M., Physica **50** (1970) 433 (Commun. Kamerlingh Onnes Lab., Leiden No. 380*b*).
20) Fiutak, J. and Van Kranendonk, J., Can. J. Phys. **40** (1962) 1085; **41** (1963) 21.
21) Prangsma, G.J., Borsboom, L.J.M., Knaap, H.F.P., Van den Meijdenberg, C.J.N. and Beenakker, J.J.M., Physica **61** (1972) 527 (Commun. Kamerlingh Onnes Lab., Leiden No. 395*a*).
22) May, A.D., Degen, V., Stryland, J.C. and Welsh, H.L., Can. J. Phys. **39** (1961) 1769.
23) Moraal, H., Physica **73** (1974) 379.